X-ray photoemission studies of diamond, graphite, and glassy carbon valence bands*

F. R. McFeely, S. P. Kowalczyk, L. Ley, R. G. Cavell,† R. A. Pollak,‡ and D. A. Shirley
Department of Chemistry and Lawrence Berkeley Laboratory, University of California, Berkeley, California 94720
(Received 26 December 1973)

The high-resolution x-ray photoemission spectra (XPS) of the total valence bands of atomically clean diamond, graphite, and glassy carbon, obtained with monochromatized Al $K\alpha$ radiation, are reported and discussed. By comparing valence-band and carbon-1s photoelectron kinetic energies, the XPS valence-band spectra $I'(E)$ of diamond and graphite were rigorously affixed to the same energy scale as earlier K x-ray emission spectra $\mathcal{I}(E)$. The two spectra—$I'(E)$ and $\mathcal{I}(E)$—have very different energy dependences of intensity because selection rules and cross-section ratios render $\mathcal{I}(E)$ sensitive only to $2p$ character and $I'(E)$ far more sensitive to $2s$ character. Taken together, $I'(E)$ and $\mathcal{I}(E)$ show that the fractional p character in the diamond valence band increases from $\sim 16\%$ at the bottom of the band to $\sim 92\%$ at the top, with an average hybridization of $\sim s^{1.2}p^{2.8}$. The spectra agree well with the density of states of Painter *et al.*, but indicate a valence-band width of 24.2(10) eV rather than their 20.8 eV. The C(1s) binding energy of 284.68(20) eV in graphite agrees well with a recent theoretical estimate of 284.4(3) eV by Davis and Shirley. Analysis of $I'(E)$ and $\mathcal{I}(E)$ for graphite resolves the valence bands cleanly into σ and π bands, with the spectrum $I'(E)$ of the former resembling that of diamond, but with a stronger $2s$ admixture (sp^2 vs sp^3). The XPS cross section of the (p_z) π bands was very low, as expected by symmetry. The bandwidth of 24(1) eV somewhat exceeded Painter and Ellis's calculated value of 19.3 eV. Glassy carbon showed an $I'(E)$ between that of diamond and graphite, consistent with an amorphous lattice containing both trigonal and tetrahedral bonds.

I. INTRODUCTION

The element carbon is in many respects unique among the group-IV elements in its solid-state properties. In its diamond modification it structurally resembles the small-band-gap tetrahedral semiconductors silicon, germanium, and grey tin, while it is a very good insulator, in contrast to these materials. At ordinary temperatures and pressures, however, the thermodynamically stable form of carbon is not diamond, but graphite, a semimetallic form without an analog in the group-IV series. It is of interest to compare the valence bands of the two forms of carbon because the different coordination—trigonal in graphite and tetrahedral in diamond—suggests substantial differences in their chemical bonding. While the simple tight-binding description of these two forms in terms of sp^2 and sp^3 bonding must be greatly modified to provide a realistic band structure, vestiges of s and p character in the bands should still be manifest through cross-section modulation in the photoemission spectrum. This effect was discussed in an earlier paper on the photemission spectrum of diamond.[1] In the present paper the valence-band x-ray photoemission spectra (XPS) of graphite and glassy carbon are reported. These spectra, together with the earlier diamond spectrum, are compared and discussed in terms both of valence-band densities of states and the relative effects of cross-section modulation in the three lattices. Comparisons are made with the lower-resolution XPS studies of several forms of carbon by Thomas *et al.*[2]

Experimental procedures are given in Sec. II. Results are presented in Sec. III and discussed in Sec. IV. Conclusions are given in Sec. V.

II. EXPERIMENTAL

The diamond sample was a single crystal,[3] and the graphite sample was part of a crystal used previously as an x-ray monochromator.[4] The glassy-carbon sample was in the form of a polished disk-shaped ingot.[5] In order to prevent contamination by hydrocarbons and/or oxygen, the samples were cleaved or fractured under dry nitrogen in a glove bag and inserted directly into a Hewlett-Packard 5950A ESCA spectrometer at 8×10^{-9} Torr without exposure to the atmosphere. They were then irradiated with monochromatized Al $K\alpha$ radiation (1486.6 eV) and the ejected photoelectrons were energy analyzed.

Energy conservation gives for the apparent binding energy of an electron

$$E_B^{\text{app}} = h\nu - K - e\phi_{\text{sp}} + e\psi \quad ,$$

where K is the measured kinetic energy of the photoelectron, ϕ_{sp} is the spectrometer work function and ψ is the Volta potential due to charging of the sample. The factors governing the magnitude of the Volta potential and its effect on the spectra have been discussed by Ley *et al.*[6] We note here that in our spectrometer, sample charging merely shifts the apparent binding energies by a constant amount and does not detectably broaden the spectral features.

The problem of obtaining an adequate reference level for the assignment of binding energies in these samples is especially difficult. In a large band-gap insulator such as diamond, appreciable charging (~6 eV) occurs. Attempts to reference the binding energies relative to the Fermi energy of a thin layer of gold evaporated onto the sample surface have proved to be inadequate, because the position of the Fermi energy determined in this way may not be intrinsic or reproducible.[6] All binding energies in diamond are therefore given with respect to an arbitrary zero point. This point was chosen to be the top of the valence bands, obtained by a linear extrapolation of the region of maximum negative slope on the leading edge of the valence bands to the background count level. Since the onset of photoemission is sharp, this point could be located with reasonable precision.

Graphite is a semimetal and thus has no band gap. The intrinsic conductivity prevents it from charging and the Fermi level is well defined at the top of the valence band. A Fermi edge was indeed observed in our spectra and binding energies are given with respect to it; however, the low intensity in this region leads to unavoidable inaccuracies in this assignment.

Glassy carbon is, in principle, an even more difficult case, since it does not have a well-defined band structure. Furthermore, its photoemission intensity at low binding energies is even lower than in the case of graphite. In order to have a well-defined reference energy for the purposes of our discussion, we aligned the centroids of the strongest valence-band peaks in graphite and glassy carbon and adopted the assigned position of E_F in graphite as the zero of energy in glassy carbon.

III. RESULTS

In Fig. 1 are shown the spectra of diamond, crystalline graphite, microcrystalline graphite, and glassy carbon. The intensity curves $I'(E)$ have been obtained from the raw spectra by the application of a correction for inelastic scattering. The correction was made by assuming that the inelastic loss spectrum could be approximated from a discrete loss structure determined by folding a response function obtained from the inelastic structure of the C-1s line with the valence-band structure.

An inspection of the spectra in Fig. 1 reveals that all four samples display the same gross structure. Each spectrum shows (i) a fairly broad, intense peak located between 16 and 21 eV, hereafter referred to as peak I, (ii) a narrower, less intense peak located at about 10 to 15 eV (peak II), and (iii) a very broad and decidedly weaker structure, extending from 10 to 13 eV to the cutoff energy ("peak" III). There are, however, easily noticeable

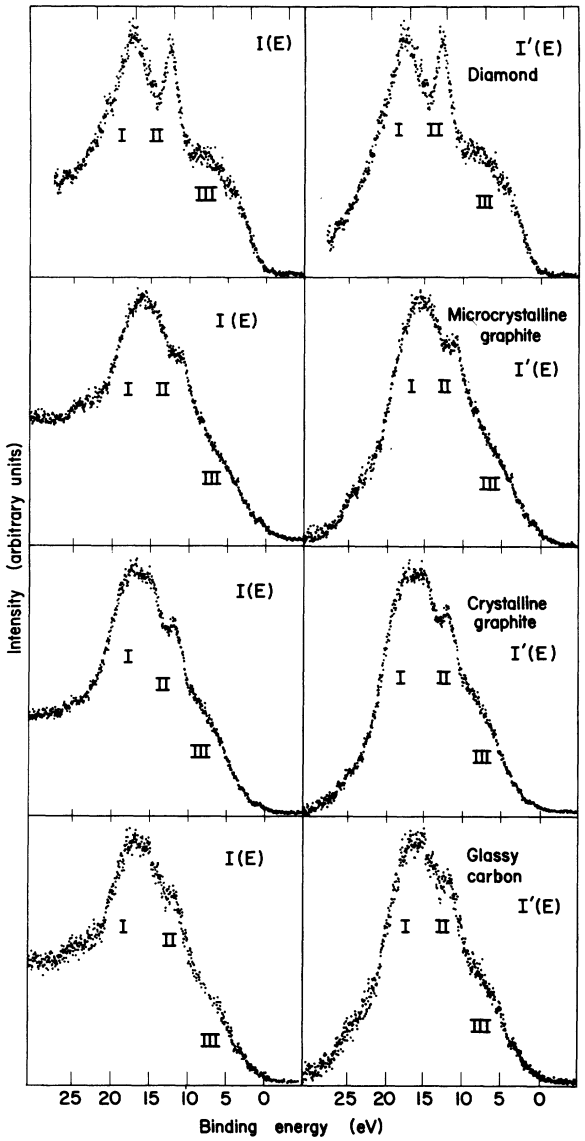

FIG. 1. Valence-band XPS spectra, before (left) and after (right) correction for inelastic losses, of diamond, microcrystalline graphite, crystalline graphite, and glassy carbon.

and significant differences in the spectra. Peak I in diamond is less dominant than its analog in graphite and glassy carbon. In addition, peak III arises sharply in diamond while in graphite it tails off slowly toward low binding energies. Also, in graphite there is a well-defined minimum between peaks I and II which persists even in the microcrystalline sample. This minimum is less pronounced in glassy carbon. In Sec. IV the factors accounting for these differences are discussed, and they are shown to arise from both density-of-states and photoemission cross-section effects.

The spectra reported by Thomas *et al.*[2] agreed

with ours in broad outline. Their valence bands were typically ~8 eV wider than ours and they showed no evidence of peak II in most cases. The excess width probably arose from a cruder scattering correction which systematically produces this effect: They subtracted a presumed background rather than inverting a response function. The absence of peak II in their spectra may be a consequence of surface contamination, inhomogeneous broadening due to a spread in the Volta potential, or simply lower resolution. The interpretation given below is based entirely on our spectra.

IV. DISCUSSION

To interpret the spectra in Fig. 1 properly, it is first necessary to consider the various factors which contribute to the photoemission intensity. The photoemission intensity at a given energy E may be written as

$$I(E) \propto \rho^i(E)\,\rho^f(\hbar\omega - E)\,\sigma(\hbar\omega, E) \quad , \tag{1}$$

where $\rho^i(E)$ is the density of initial states in the crystal, $\rho^f(\hbar\omega - E)$ is the density of final states of the system including the final state of the photoelectron, and σ is the cross section for the process. A one-electron-transition model is of course assumed in this discussion. At ~1480 eV the conduction bands of these crystals are expected to be very free-electron-like and thus featureless, reducing the intensity expression to

$$I(E) \propto \rho^i(E)\,\sigma(\hbar\omega, E) \quad . \tag{2}$$

In carbon, the cross-section term is extremely important, as $\sigma(\hbar\omega, E)$ is a very strong function of E in the valence-band region.

It can be shown[7,8] that the cross section for photoemission from a state ψ_k may be written as

$$\sigma_k \propto |\langle \psi_k | PW(q) \rangle|^2 \quad , \tag{3}$$

where $PW(q)$ denotes a plane wave of wave vector q. In deriving this expression, it is necessary to assume the electric-dipole approximation, the Born-Oppenheimer approximation, a frozen-orbital approximation for the photoemission process, and finally that the continuum state of the photoelectron may be represented by a plane wave. This last approximation is rather dubious in principle since it violates the fundamental requirements of orthogonality. However, at large q the error introduced by it should not be serious.

The only problem remaining in the calculation of σ_k is our lack of knowledge about the band state ψ_k, which is the object of study. Since atomic cross sections may be determined unambiguously either by experiment or calculation, we shall adopt the approach of relating the band-state cross sections to their atomic components. This is in principle a difficult undertaking, since the free-atom states are eigenstates of the angular momentum, while the band states are eigenstates of the linear momentum. However, Bloch's theorem states that an eigenfunction of the nth band of momentum $\hbar k$ may be written

$$\psi_{n\vec{k}}(\vec{r}) = u_{n\vec{k}}(\vec{r})\, e^{i\vec{k}\cdot\vec{r}} \quad , \tag{4}$$

where $\vec{k}$ lies within the first Brillouin zone and $u_{n\vec{k}}(\vec{r})$ is a function with the periodicity of the lattice, depending only parametrically on $\vec{k}$.

For the case of a linear one-dimensional lattice with lattice constant a, $-\pi/a < k \leq \pi/a$. Since $\lambda = 2\pi/k$, the minimum wavelength of the phase factors in Eq. (4) will be $\lambda_{\min} = 2a$. The extension to three-dimensional lattices is clear. The importance of this result lies in the form of the overlap integral (3). This integral can be large if the curvature of the plane wave matches that of the Bloch state. Since the de Broglie wavelength of an electron ejected from the valence bands is ~0.32 Å, there can be no significant contribution from the phase factor of the Bloch state. The overwhelming contribution to this integral must come, then, from the overlap of the plane wave with $u_{n\vec{k}}(\vec{r})$, the periodic part of the Bloch function.

In the limit of totally noninteracting electrons in a lattice, the $u_{n,\vec{k}}(\vec{r})$ reduce to the atomic functions, losing their parametric dependence on $\vec{k}$. In the actual crystal, $u_{n,\vec{k}}(\vec{r})$ will resemble some linear combination of atomic functions to a very high degree near the nuclei, since in these regions the perturbation due to the presence of the other atoms is relatively small. Furthermore, it is precisely in this region near the nuclei that the radial nodes in the wave function can match the curvature of the plane wave, yielding a large contribution to the integral. Therefore, a band constructed from states of the type $\psi_{\vec{k}} = \phi_{2s}(\vec{r})\, e^{i\vec{k}\cdot\vec{r}}$, for example, should be expected to show qualitatively the same cross-section behavior as an assembly of noninteracting $2s$ states. One can therefore regard the cross section of the band state as the sum of the cross sections of its principal atomic components. Thus, if a band is formed largely out of atomic s and p orbitals the photoemission cross section should reflect the relative extent of the s and p character of the band.

In carbon, the effect of cross-section modulation in the valence bands is particularly large. The valence bands arise mostly from the $2s$ and $2p$ atomic states, and the cross-section ratio for photoemission by Al $K\alpha_{12}$ x-rays is $\sigma(2s)/\sigma(2p) \approx 13$.[9] The reason for this large ratio is that the $2s$ atomic function has one radial node while the $2p$ state has no radial nodes. The great increase in curvature provided by the $2s$ node allows for much larger overlap with the $\lambda = 0.32$-Å plane-wave-like final

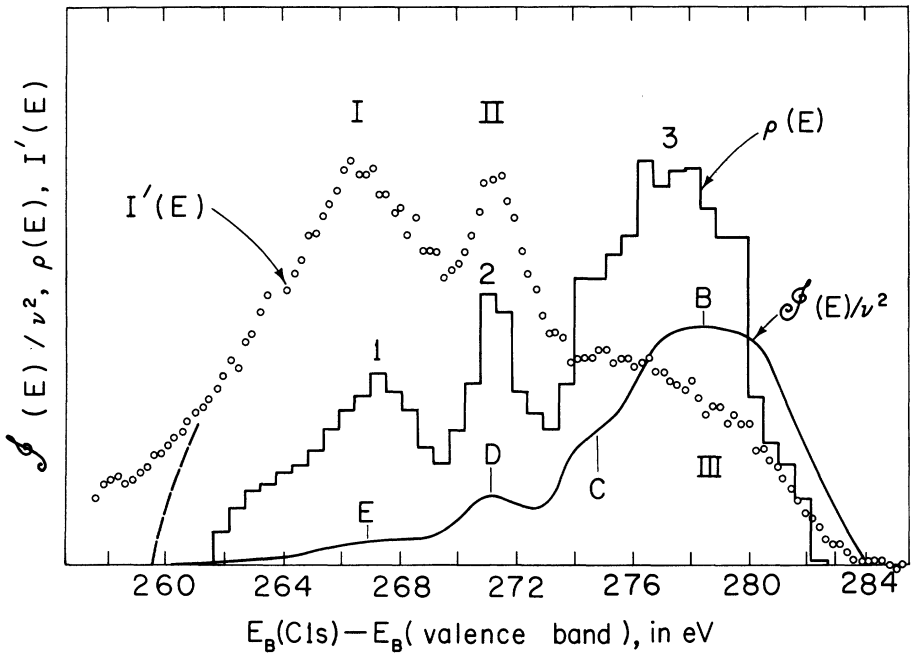

FIG. 2. Comparison for diamond of the XPS spectrum $I'(E)$ (this work), the K x-ray emission spectrum $\mathcal{g}(E)/\nu^2$ (Ref. 11), and the calculated density of states (Ref. 10). Characteristic features are denoted by roman numerals for $I'(E)$, arabic numerals for $\rho(E)$, and letters for $\mathcal{g}(E)/\nu^2$. Abscissa pertains to $I'(E)$ and $\mathcal{g}(E)/\nu^2$, as described in text; $\rho(E)$ was drawn by aligning peak 2 with peak II in $I'(E)$. Ordinates are linear and start from zero. Dashed line indicates extrapolation of $I'(E)$ to zero at the bottom of the valence bands to eliminate an artificial tail.

state. With these effects in mind the valence-band spectra of each form of carbon can now be examined.

A. Diamond

The XPS spectrum of diamond has been discussed earlier[1] in connection with cross-section modulation and the theoretical density of states given by Painter *et al.*[10] We shall briefly discuss this spectrum again here for two reasons. First, it provides a useful framework for understanding the glassy-carbon results; and second, we have recently realized that the valence-band spectrum can be nicely related to the x-ray emission spectrum in a way that obviates the necessity of establishing a fiducial energy such as E_F or the top of the valence bands. Figure 2 shows our XPS spectrum $I'(E)$, the K emission spectrum $\mathcal{g}(E)/\nu^2$ of Wiech and Zöpf,[11] and the density of states[10] $\rho(E)$ of diamond. The abscissa is the K x-ray emission energy, $E(1s-v)$, to which we have referred the valence-band XPS spectrum in a completely rigorous way by using the relation

$$E(1s-v)=E_B(1s)-E_B(\text{valence}) \ ,$$

where the two quantities E_B are binding energies with any common reference. Our reference was the Fermi energy of an evaporated gold layer.[1] Thus, for example, the sharp middle peak of the XPS valence-band spectrum (peak II) falls at 271.2 eV on the $E(1s-v)$ scale, the difference between $E_B^F(1s)=284.44(7)$ eV and $E_B^F(\text{II})=13.2(2)$ eV.[1]

Although the above relation is rigorous and straightforward, there exists in the literature a strong tendency to discuss x-ray emission and XPS results in terms of initial-state one-electron orbital energies, ϵ. Since orbital energies are computational artifacts rather than observables, confusion may arise in the comparison of XPS and x-ray emission spectra owing to the presence of (different) many-body relaxation effects. This problem need never arise, however, if the total energies of the system are considered. Figure 3 shows the energy-level structure of the diamond lattice according to this description. Because x-ray emission connects the two states that are studied by photoemission—the $1s$ hole state and the valence-band hole state—the energies should match up, and indeed this appears to be the case in Fig. 2. Referring to that figure we note that feature E in the x-ray spectrum corresponds quite well to our peak I, and Peak D to our peak II. Peak B and shoulder C can be interpreted as corresponding to the broad "peak" III in the XPS spectrum. Especially pleasing is the agreement between the positions of the top of the valence band, obtained by extrapolating peaks B and III. These fall at energies of 283.7 eV (peak III) and 283.9 eV (peak B). The valence-band-peak energies in diamond therefore appear to be on a very firm experimental basis. The energy dependence of the intensities of the x-ray emission and XPS spectra, $\mathcal{g}(E)$ and $I'(E)$, are very different, however. To interpret this observation let us relate $\mathcal{g}(E)$ and $I'(E)$ to the electronic band structure of diamond.

With two atoms per unit cell, diamond has eight valence electrons filling four bands. The lowest band, which is wide and s-like, gives rise to peak

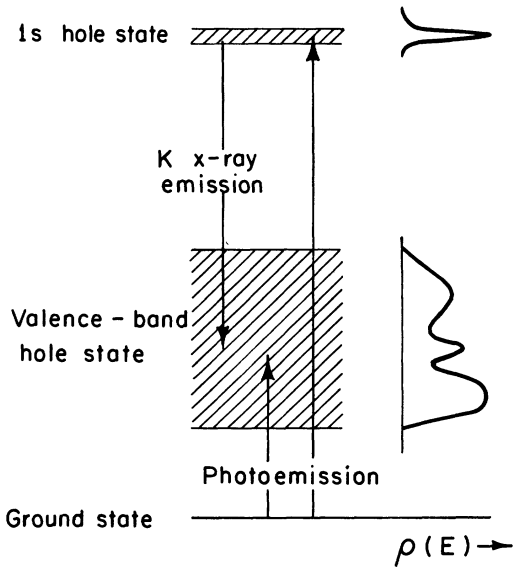

FIG. 3. Relation between photoemission valence-band spectra and x-ray emission energies discussed in text. Because these are excited (hole) states the relationship between spectral *energies* is rigorous. *Intensities* can vary quite differently across the valence band, however, because the two spectroscopies involve different transitions. Thus, in Fig. 2 the s-like bands are emphasized in XPS and the p-like bands in K x-ray emission relative to $\rho(E)$.

1 in the density of states,[11] to peak I in the XPS spectrum, and probably to feature E in the x-ray emission spectrum. The high cross section of the C($2s$) orbital for photoemission at this energy[1] greatly enhances the prominence of peak I, while feature E in $\mathcal{I}(E)/\nu^2$ is suppressed because the $2s \rightarrow 1s$ transition is forbidden in the K emission spectrum.

The second valence band is degenerate with band 1 along the line X-Z-W in the Brillouin zone.[10] It contains a strong mixture of s and p character. Because peak II in $I'(E)$ and peak D in $\mathcal{I}(E)/\nu^2$ arise largely from this second band, they are enhanced (suppressed) to an intermediate extent relative to peak 2 in $\rho(E)$ by cross-section modulation.

More dramatic changes of intensity are observed in peaks III and B. This is attributable to the stronger p character of bands 3 and 4, which largely comprise peak 3 in $\rho(E)$. For $2p$ electrons K x-ray emission is completely allowed, while the cross section for x-ray photoemission is lower by a factor of 13 than that of a $2s$ electron.

Although the agreement between the XPS spectrum and $\rho(E)$ as given by Painter *et al.*[10] was described earlier as "excellent,"[1] there was at that time some uncertainty as to how the relative energies of $I'(E)$ and $\rho(E)$ should be compared. With the aditional support of the x-ray emission spectrum $\mathcal{I}(E)/\nu^2$, and particularly in view of the agreement between $\mathcal{I}(E)/\nu^2$ and $I'(E)$ we can make a more critical comparison of theory and experiment. To do this we aligned peak 2 in $\rho(E)$ with peaks D and II, which agreed well with one another [although $\rho(E)$ has the same size energy scale in Fig. 2 as do $\mathcal{I}(E)/\nu^2$ and $I'(E)$, the transition energy on the abscissa of course does not apply to $\rho(E)$]. The theoretical $\rho(E)$ histogram then appears to be somewhat narrower than the experimental curves, both over-all and with regard to the energy separation between characteristic features. Thus the total valence-band width is 24.2 ± 1.0 eV experimentally, with most of the uncertainty arising from the extrapolation of $I'(E)$ to zero intensity at the bottom of the bands. Even after scattering corrections are made, valence-band XPS spectra tend to show "tailing" at the low-energy end. We believe that this arises from imperfect scattering corrections rather than valence-band structure because theoretically the first band decreases smoothly and parabolically in energy as it approaches the band minimum at Γ in the Brillouin zone and thus $\rho(E)$ should decrease rapidly. Accordingly we have sketched in a dashed line in Fig. 2 that represents what we believe to be the shape of $I'(E)$ if scattering were fully accounted for. This line intersects the abscissa at an energy of 259.6 eV with an estimated accuracy of 1 eV or better. The bandwidth of 24.2 ± 1.0 eV was obtained by subtracting this energy from that of the top of the bands, 283.8 ± 0.1 eV. The calculations of Painter *et al.*[10] gave a bandwidth of about 20.8 eV. In Table I the energies of several features are listed, using the top of the valence bands as reference.

In a more qualitative vein it is of interest to derive information about s-p hybridization from the diamond valence-band spectrum. The tetrahedral structure of diamond leads naturally to attempts to describe its bonding in terms of sp^3 hybridization. While this approach has some validity at Γ

TABLE I. Positions of characteristic points in the diamond valence bands (in eV).

Feature	E(x-ray)[a,b]	E(XPS)[b,c]	E(theor)[b,d]
Midpoint of top peak (3, B, III)	5.5	~6	4.3
Shoulder (C)	9.0	···	7.5
Second peak (2, D, II)	12.9	12.6	11.0
Minimum	···	14.2	12.8
Bottom peak (I, E, 1)	~17	17.1	15.0
Bottom of valence bands	···	24.2	20.8

[a]Reference 11.
[b]Energy below top of valence band.
[c]This work.
[d]Reference 10.

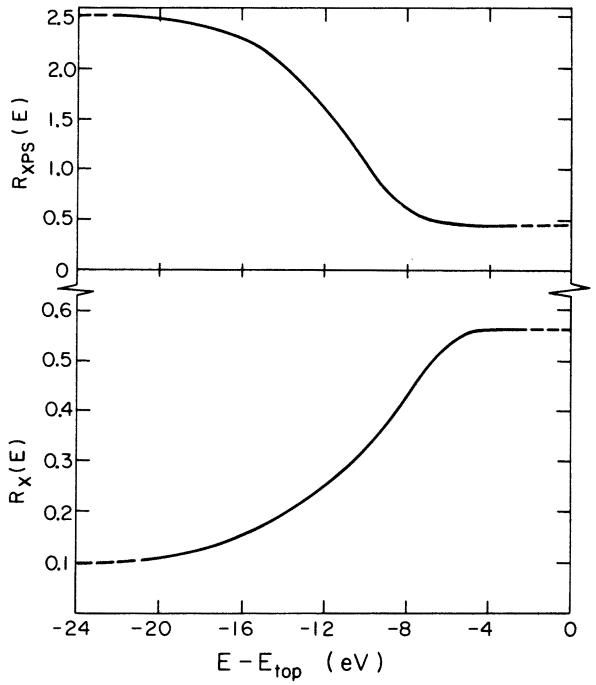

FIG. 4. Plot for the diamond valence bands of the ratios $R_{XPS}=I'(E)/\rho(E)$ (top panel) and $R_X(E)=(g(E)/\nu^2)/\rho(E)$.

in the Brillouin zone, the crystal symmetry requires the linear momentum $\vec{k}$, rather than angular momentum, be a good quantum number. For this reason an atomic-orbital basis set, and especially one that is limited to $2s$ and $2p$ functions, is inadequate to describe the valence bands. Still, both XPS and K x-ray emission are most sensitive to those parts of the valence-band wave functions nearest the nucleus, where they are most like atomic functions. These methods are thus expected to give as good an index of $2s$ or $2p$ character as is available. The XPS spectrum $I'(E)$ was compared to $\rho(E)$ alone earlier to give a rough measure of s and p character across the valence-band region. With the additional intensity information and a more reliable reference energy provided by the x-ray emission data, we can now carry this analysis further.

First we make the qualitative observation that, while Fig. 2 indicates mainly s character at the bottom of the valence bands and mainly p character at the top, there is clear evidence for considerable s-p mixing throughout. The finite value of $g(E)/\nu^2$ in feature E denotes some p character. On the other hand, the ratio

$$\frac{[I'(E)/\rho(E)]_{\text{peak I}}}{[I'(E)/\rho(E)]_{\text{peak III}}} \approx 5 \tag{5}$$

is significantly less than $\sigma(2s)/\sigma(2p)=13$, the value expected if peak I were pure $2s$ and peak III pure $2p$ in character.

To carry this analysis further we defined the ratios

$$R_{XPS}(E) \equiv I'(E)/\rho(E) \ ,$$
$$R_X(E) \equiv [g(E)/\nu^2]/\rho(E) \ . \tag{6}$$

The values of $R_{XPS}(E)$ and $R_X(E)$, as deduced from the data in Fig. 2, are plotted in Fig. 4. Since $\rho(E)$ did not line up exactly with the two spectra, it was necessary to expand the energy scale of $\rho(E)$ slightly and to smooth the rather rough curve given by point-by-point calculations of $R_{XPS}(E)$ and $R_X(E)$. This may result in the loss of some meaningful fine structure.

To extract the fractional s and p characters from the ratios in Fig. 4, we define fractions of s and p character, $f_s(E)$ and $f_p(E)$, and assume $f_s(E)+f_p(E)=1$ for all E. Since the K x-ray emission cross section is zero for $2s$ electrons, we can write

$$f_p(T)/f_p(B)=R_X(T)/R_X(B)=5.6 \ , \tag{7}$$

where the number 5.6 was taken from Fig. 4 and T and B denote the top and bottom of the bands. Invoking the free-atom XPS cross-section ratio of 13, we have

$$\frac{f_p(B)+13f_s(B)}{f_p(T)+13f_s(T)}=\frac{R_{XPS}(B)}{R_{XPS}(T)}=5.86 \ . \tag{8}$$

Simultaneous solution of these equations gives

$$f_p(B)=0.16 \ , \quad f_p(T)=0.92$$

as the fractional p mixing at the bottom and top of

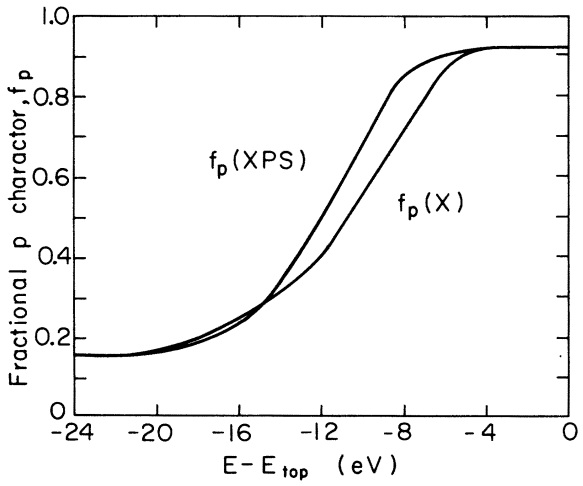

FIG. 5. Fractional p character for the diamond valence bands. The end points were derived from XPS and K emission data together, as described in text. The intermediate values were then derived separately from XPS and K emission spectra.

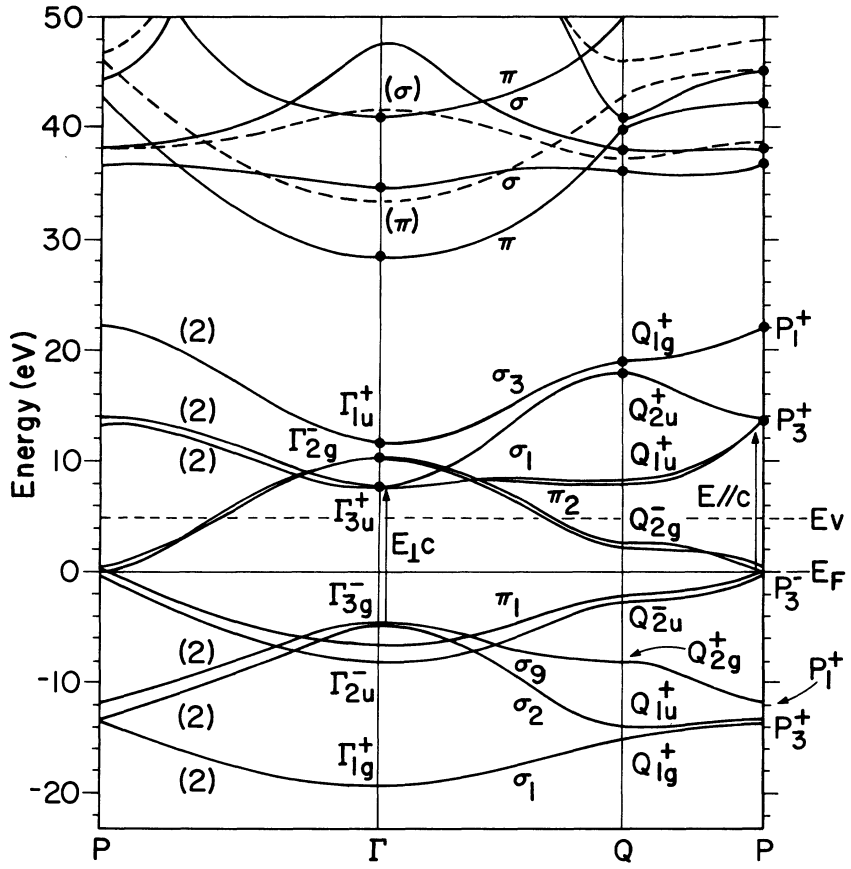

FIG. 6. Graphite band structure, after Painter and Ellis. Symmetry designations are based on the modified version quoted by Willis and Fitton (Ref. 13).

the diamond valence bands. By comparing $R_{\mathrm{XPS}}(E)$ and $R_X(E)$ separately with these two end points, we can derive two estimates of the energy dependence of f_p that are based mainly on XPS and x-ray emission spectra, respectively. These are shown in Fig. 5. The two estimates of f_p show satisfactory agreement, especially considering the difficulty of estimating f_p. At a more speculative level of interpretation, we can evaluate the mean fractional p character of the diamond valence bands as

$$\bar{f}_p = \frac{\int f_p(E)\,\rho(E)\,dE}{\int \rho(E)\,dE} = 0.695 \quad , \tag{9}$$

which implies a configuration of $s^{1.2}p^{2.8}$ for diamond, in good agreement with chemical intuition, which would favor sp^3 over s^2p^2.

B. Graphite

The graphite structure has layers of fused hexagonal rings, with four atoms in the primitive cell.[12] Its valence-band structure has eight filled bands instead of four. A band structure calculated by Painter and Ellis[13] is shown in Fig. 6. This *ab initio* variational calculation used a linear-combination-of-atomic-orbitals (LCAO) basis set of Bloch states,

$$\chi_i(\vec{k},\vec{r}) = \sum_\nu e^{i\vec{k}\cdot\vec{R}_\nu} u_i(\vec{r}-\vec{R}_\nu-\vec{U}_i) \quad , \tag{10}$$

where U_i is a vector specifying the atomic position within the unit cell, and u_i is an atomic function. The matrix elements of the Hamiltonian were evaluated without resorting to tight-binding approximations.

The layered nature of the graphite structure causes the bands to be grouped into two distinct classes consisting of six σ bands and two π bands. The π bands are formed largely from the functions $u_i = 2p_z$, while the σ bands are formed from the remaining orbitals.

The valence-band XPS spectrum of graphite is shown in Fig. 7, together with the K x-ray emission spectrum of Chalklin.[14] The C(1s) binding energy relative to the Fermi level, $E_B^F(\mathrm{C}(1s))$ = 284.68(20) eV, was used to set the valence-band XPS spectrum on the same scale as the K x-ray emission spectrum. The value of $E_B^F(\mathrm{C}(1s))$ has recently been estimated theoretically by Davis and Shirley[15] as $E_B^F = 284.4(3)$ eV (after correction for a work function of 4.6 V). This excellent agreement is very encouraging, especially so because a rather large relaxation-energy term was involved in the theoretical estimate.

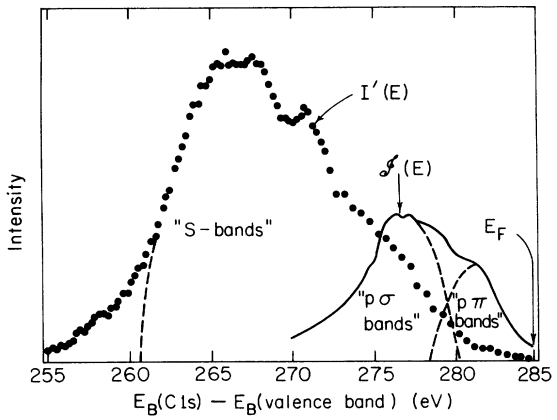

FIG. 7. Graphite valence-band XPS spectrum $I'(E)$ and K x-ray emission spectrum $\mathcal{J}(E)$ (Ref. 14). The ordinate is linear and begins at zero. The dashed line at the bottom of the bands is an extrapolation to eliminate artificial tailing. The other dashed lines denote a resolution of the p-band structure as described in text. The Fermi energy falls at 284.68(20) eV.

In contrast to diamond, peak I in the graphite structure is even more dominant, with a broad, flat top. This peak arises from the two nearly degenerate s-like σ_1 bands. Because a set of p-like atomic orbitals, the $2p_z$'s, are largely unmixed with the other bands, one would expect peak I to arise from purer s-like states than its analog in diamond. This explains, at least qualitatively, its greater relative intensity. The width of this feature (~5 eV) corresponds reasonably well with the value of 5.90 eV calculated by Painter and Ellis for the width of the σ_1 bands, while its flat top may arise from the shallowly sloping σ_1 and σ_2 bands between Q and P in the Brillouin zone.

Proceeding to lower binding energies we find a small peak located at 13.8 eV below E_F and separated from the σ_1 peak by a distinct minimum. This peak may be interpreted in light of the band-structure calculation as being due to the high density of states near the point P_1^+ in the Brillouin zone, with the width of the valley reflecting the separation of the two σ_2 and two σ_3 bands at the symmetry point P. This peak drops off very sharply on the low-binding-energy side, reflecting the relatively steep rise of the σ_2 and σ_3 bands in this region. There is then an inflection in this descent in the region E_F − (8 to 12) eV. In this energy region the K emission spectrum begins to show appreciable intensity. the σ and π bands are labeled after Tomboulian[16] according to the calculations of Coulson and Taylor.[17] From $E_F - 10$ eV up to E_F, corresponding to a K emission energy range of 275–285 eV, the XPS spectrum and the K emission spectrum are discussed together below.

From $E_F - 8$ eV to $E_F - 4$ eV the XPS intensity $I'(E)$ decreases very rapidly. We attribute this to the exhaustion of the σ_2 and σ_3 bands at ~$E_F - 4$ eV.[13] These bands, but not the higher π bands, can have some $2s$ character and hence a relatively large cross section. The rapid decrease in $I'(E)$ is largely due to the location of the top of the σ_2 and σ_3 bands at Γ, where the phase-space factor in the Brillouin zone goes to zero. The K emission spectrum of the σ bands would probably behave in a qualitatively similar manner if it could be observed alone, but the $p\pi$ bands have an appreciable intensity in $\mathcal{J}(E)$, and the $p\pi$-bands peak appears as a strong shoulder in the $p\sigma$ peak. The drop of the XPS intensity to a low value at $E_F - 4$ eV constitutes strong independent evidence that the shoulder in $I(E)$ is in fact attributable to $p\pi$ bands, on the basis of cross-section variation. The $p\pi$-peak location at E_F − (3 to 4) eV in $I'(E)$ is in fairly good agreement with the energy E_F − (2 to 3) eV for the flat region of the π bands near Q in the band-structure calculation.[13] Both $\mathcal{J}(E)$ and $I'(E)$ indicate a maximum in the σ-band density of states at ~$E_F - 8$ eV. This is probably related to the flat region of the σ_3 band near Q_{2g}^+, which lies at $E_F - 7.7$ eV.[13]

The reasons for the complete reversal of cross-section ratios in $I'(E)$ and $\mathcal{J}(E)$ in graphite are simple and illuminating. As discussed above the XPS cross section for $2s$ photoemission is about 13 times that for $2p$ photoemission. The general decrease of $I'(E)$ with energy from the bottom of the valence bands to ~$E_F - 5$ eV, where the σ bands end, may be attributed to a decrease in the $2s/2p$ ratio as in diamond. It is interesting to note the resemblance between $I'(E)$ for this σ-band portion of the graphite valence bands and $I'(E)$ for the diamond valence bands (Fig. 2). This similarity is pleasing, because the two spectra correspond respectively to

TABLE II. Tentative comparison of positions of characteristic features and symmetry points in graphite valence bands (in eV below E_F).

Experimental feature	Energy	Theoretical feature	Energy[a]
π-band peak	3–4	flat π band near Q	2–3
top of σ bands	~5	Γ_{3g}^-	4.5
σ-band peak	8 ± 1	flat σ_3 band near Q_{2g}^+	~7.7
sharp peak	13.8	P_1^+	11.5
flat-top σ peak	17–19	P_3^+, Q_{1g}^+	13,15
bottom of bands	24	Γ_{1g}^+	19.3

[a]These numbers were read from the plots of Painter and Ellis (Ref. 13).

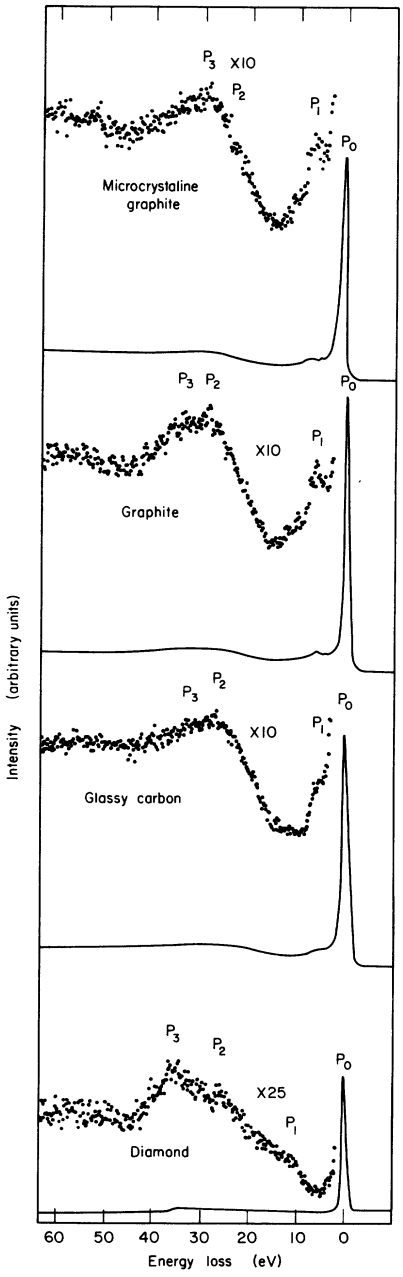

FIG. 8. Carbon 1*s* and characteristic energy-loss spectra of microcrystalline graphite, graphite, glassy carbon, and diamond. The carbon 1*s* peaks P_0 have been aligned.

two- and three-dimensional lattices of carbon atoms. As noted above, even the increased dominance of the $I'(E)$ features in the bottom of the band in graphite relative to diamond can be explained as arising from a richer mixture of nominal *s* character in the σ framework (sp^2 vs sp^3). The *K* emission spectrum is sensitive only to 2*p* character; thus that part of $g(E)$ that arises from $p\sigma$ bands increases as $I'(E)$ decreases near the top of the σ bands, as was the case for diamond.

A further, more striking extension of the reversal in cross section between $I'(E)$ and $g(E)$ is apparent for the $p\pi$ bands. The *K* emission cross section for the $2p_z$ electrons that constitute the $p\pi$ bands is expected to be about the same as that of the 2*p* electrons in the σ bands. This expectation is borne out qualitatively by the relative intensities of the $p\sigma$-band and $p\pi$-band peaks in Fig. 7 (the simple $sp^2 + p_z$ model would give this intensity ratio as $p\sigma/p\pi \sim 2$). The cross section of the $p\pi$ bands for photoemission is very low, however. Only part of this low value can be attributed to the absence of *s* character in the $p\pi$ bands. The rest may arise from changes in the p_z wave functions at large radii due to the delocalized nature of the $p\pi$ orbitals.

Table II compares energies of graphite valence-band symmetry points derived from the spectra in Fig. 7 with those calculated by Painter and Ellis.[13] The comparison is somewhat tentative because no calculated density of states is available. However, it appears that we now have a good qualitative understanding of the graphite valence bands. There is some quantitative disagreement between experiment and theory: In particular, our 24-eV bandwidth substantially exceeds the 19.3-eV value of Painter and Ellis. Two earlier estimates of the valence-band width should be commented upon at this point. The agreement between their bandwidth of 19.3 eV and the *K* emission value of 18 eV noted by Painter and Ellis[13] is not valid because the latter applies only to *p* bands (Fig. 7). Also, the bandwidth of 31 ± 2 eV reported by Thomas *et al.*[2]

TABLE III. Carbon characteristic energy losses (eV).

	P_1	P_2	P_3
	Graphite		
XPS	6.3(1)	28.1(3)	33.3(3)
Other measurements[a]	7.2	24.9	···
Calc.	7.5[a], 12.5[b]	25.1	···
	Microcrystalline graphite		
XPS	5.6(2)	22.0(4)	30.3(4)
Other measurements[a]	···	···	···
Calc.	6.7–7.2	22.3–24.1	
	Glassy carbon		
XPS	5.6(2)	26.5(3)	31.6(3)
Other measurements[c]	5.6	21	···
Calc.	6.1	20.3	···
	Diamond		
XPS	11.3(2)	25.4(2)	34.1(3)
Other measurements[d]	12.5	23	31
Calc.	12.5	···	31.1

[a]Reference 24.

[b]W. Y. Liang and S. L. Cundy, Phil. Mag. 19, 1031 (1969).

[c]Reference 22.

[d]Reference 23.

differs from our result mainly because of different data analyses: Their raw data agree reasonably well with ours if differences in resolution are taken into account.

C. Glassy carbon

In examining the valence-band spectrum of glassy carbon, the following observations can be made: (i) The spectrum resembles that of graphite more than diamond in the region of peak III, showing a gradual decrease in intensity rather than a sharp cutoff. (ii) The total width of the intense part of $I'(E)$ is nearer that of graphite than that of diamond. Defining this width W as the energy separation between the points in $I'(E)$ of half the maximum height on the low-energy side and of quarter height on the high-energy side, we find $W = 15.5$ eV (graphite), 18 eV (diamond), and 16 eV (glassy carbon). (iii) Peak I is intermediate in relative intensity between diamond and graphite. (iv) The valley between peaks I and II is filled in.

It is actually not surprising that the XPS spectrum of the amorphous material should resemble the crystalline cases so closely. As Weaire and Thorpe[18] have pointed out and numerous XPS experiments have demonstrated, the gross features of the density of states depend on atomic properties and the short-range order in the crystal, while the long-range order is responsible for the fine structure. The filling-in of the valley between peaks I and II is an example of the kind of fine-structure change observed earlier in amorphous materials.[19,20] The other features noted above are consistent with glassy carbon possessing both trigonally and tetrahedrally coordinated carbons, with more of the former than the latter.

Figure 8 shows the XPS spectra of the carbon-1s line and its associated characteristic energy losses (CEL's) of the four carbon specimens of this study. The values of the CEL's are tabulated in Table III. A detailed study of the role of CEL's in the XPS spectra of solids is given in Ref. 21. Qualitatively the CEL's of glassy carbon resemble graphite more than diamond. This is particulary evident in P_1, which has been attributed to either an interband transition[22,23] or a collective π electron excitation.[24,25] Since diamond also has a P_1 it is more likely that P_1 is due to an interband transition rather than a collective π electron excitation. Our diamond results agree well with the reflectance experiments of Whetten.[23] Our results for graphite, microcrystalline graphite, and glassy carbon agree reasonably well with other experiments for P_1 and P_2.[22,24] However, it appears P_3 has not been previously reported for graphite and glassy carbon. Our CEL results further support the interpretation of glassy carbon as being primarily graphitic.

A number of models for the structure of glassy carbon have been proposed on the basis of x-ray diffraction data.[26–28] Our results do not rule out any of these, although they specifically support those that include both trigonal and tetrahedral bonding.

Further evidence is provided by the K emission data of Saxena and Bragg[29] who noted that the position of the K emission band in glassy carbon falls midway between that of diamond and graphite.

V. CONCLUSIONS

High-resolution XPS spectra of atomically clean diamond graphite and glassy carbon were obtained. The diamond and graphite spectra were found to agree well with band-structure calculations after photoemission cross-section effects were properly taken into account. By comparing the difference between valence-band and carbon-1s binding energies with K x-ray emission energies, the XPS and x-ray emission spectra of the diamond and graphite valence bands were rigorously placed on the same energy scale. The fractional p character increased from ~16% at the bottom of the diamond valence bands to ~92% at the top, and an average hybridization of $s^{1.2}p^{2.8}$ was derived. Comparison of XPS and x-ray emission data divided the graphite valence bands cleanly into σ and π bands, with the former being essentially a two-dimensional version of the diamond bands. Glassy carbon had an XPS spectrum between that of diamond and graphite, in agreement with the presence of both trigonal and tetrahedral coordination.

---

*Work performed under the auspices of the U. S. Atomic Energy Commission.

†Present address: University of Alberta, Edmonton, Canada.

‡Present address: IBM T. J. Watson Research Center, Yorktown Heights, New York.

[1]R. G. Cavell, S. P. Kowalczyk, L. Ley, R. A. Pollak, B. Mills, D. A. Shirley, and W. Perry, Phys. Rev. B 7, 5313 (1973).

[2]J. M. Thomas, E. L. Evans, M. Barber, and P. Swift, Trans. Faraday Soc. 67, 1875 (1972).

[3]Our diamond sample was a 1.35 carat industrial diamond obtained from West Coast Diamond Tool Co.

[4]Our graphite crystal was obtained from Picker Corp. where it had been used as an x-ray monochromator.

[5]Our glassy-carbon sample was a gift of Professor R. H. Bragg.

[6]L. Ley, R. A. Pollak, F. R. McFeely, S. P. Kowalczyk, and D. A. Shirley, Phys. Rev. B 9, 600 (1974).

[7]I. G. Kaplan and A. P. Marklin, Dokl. Akad. Nauk SSSR 184, 66 (1968) [Sov. Phys.-Dokl. 14, 36 (1969)].

[8]L. L. Lohr, Jr. and M. B. Robin, J. Am. Chem. Soc. 92, 7241 (1969).

[9]U. Gelius, in *Electron Spectroscopy*, edited by D. A. Shirley (North-Holland, Amsterdam, 1972), p. 311.

[10]G. S. Painter, D. E. Ellis, and A. R. Lubinsky, Phys.

Rev. B 4, 3610 (1971).
[11]Wiech and Zöpf, in *Electronic Density of States*, Natl. Bur. Stand. Spec. Publ. 323 (U.S. GPO, Washington, D. C., 1969), p. 335.
[12]R. W. G. Wycoff, *Crystal Structures* (Wiley, New York, 1963), Vol. 1, p. 27.
[13]G. S. Painter and D. E. Ellis, Phys. Rev. B 1, 4747 (1970). A modified version of this calculation was quoted by R. F. Willis and B. Fitton, J. Vac. Sci. Technol. 9, 651 (1972).
[14]F. C. Chalklin, Proc. R. Soc. A 194, 42 (1948).
[15]D. W. Davis and D. A. Shirley, J. Electron Spectrosc. 3, 137 (1974).
[16]D. H. Tomboulian, *Handbuch der Physik XXX*, edited by S. Flügge (Springer-Verlag, Berlin, 1957), p. 246.
[17]C. A. Coulson and R. Taylor, Proc. Phys. Soc. Lond. A 65, 815 (1952).
[18]D. Weaire and M. F. Thorpe, Phys. Rev. B 4, 2508 (1971).
[19]L. Ley, S. Kowalczyk, R. Pollak, and D. A. Shirley, Phys. Rev. Lett. 29, 1088 (1972).
[20]L. Ley, R. A. Pollak, F. R. McFeely, S. P. Kowalczyk, and D. A. Shirley, Phys. Rev. B 8, 641 (1973).
[21]R. A. Pollak, L. Ley, F. R. McFeely, S. P. Kowalczyk, and D. A. Shirley, J. Electron Spectrosc. (to be published).
[22]E. A. Taft and H. R. Philipp, Phys. Rev. 138, A197 (1965).
[23]N. R. Whetten, Appl. Phys. Lett. 8, 135 (1966).
[24]L. B. Leder and J. A. Suddeth, J. Appl. Phys. 31, 1422 (1960).
[25]Y. H. Ichikawa, Phys. Rev. 109, 653 (1958).
[26]T. Noda and N. Inagaki, Bull. Chem. Soc. Jap. 37, 1534 (1964).
[27]J. Kakinoki, Acta Crystallogr. 18, 518 (1963).
[28]K. Furukawa, J. Cryst. (Japan) 6, 101 (1964).
[29]R. R. Saxena and R. H. Bragg (private communication).